Multiloop Analysis of a Precision Pointing Spacecraft with Controlled Flexible Appendages

J. S. Pistiner,* G. T. Tseng,* and L. Muhlfelder†
RCA Corporation, Astro-Electronics Division, Princeton, N.J.

This paper describes the development and application of a multiloop frequency response analysis method to determine the stability and response to disturbances of a precision pointing earth-oriented satellite with a controlled flexible appendage. Since the spacecraft control axes are not principal axes and the driven solar array represents a flexible appendage, single-loop rigid body analysis will not yield valid stability predictions. A four-loop (roll, pitch, yaw, array) frequency-domain computer program was developed, which permits the servo designer to verify open- and closed-loop stability of the strongly coupled servos in the presence of multiple low-frequency flexible body modes. Although the approach presented here was applied to a specific satellite application, its methodology can readily be adapted to other spacecraft configurations with controlled flexible appendages.

Introduction

EVER since the unstable behavior exhibited by Explorer I, the influence of spacecraft structural flexibility on its attitude stability has attracted increasing attention. During the past decade, both the complexity and the physical size of the spacecraft flexible appendages have grown substantially. At the same time, the pointing accuracy requirements have become more and more stringent. Numerous technical articles[1-11] dealing with flexible spacecraft attitude dynamics and stability have appeared in this period. However, relatively fewer papers[12-15] addressed themselves to the problem of actually designing an active attitude control system for a complex flexible spacecraft. This paper presents a practical and economical design approach as it is applied to a rather unique spacecraft.

The Block 5D Defense Meteorological Satellite Program (DMSP) Spacecraft is a high-precision pointing, earth-oriented satellite with a servoed flexible appendage (Fig. 1). The attitude control system consists of an inertial reference with celestial updates for primary reference and of a three-axis reaction-wheel system with magnetic desaturation. An onboard computer calculates the necessary control torque commands. This computation utilizes Euler angle information derived from the attitude sensors in conjunction with computer-stored star-catalog and spacecraft ephemeris data.

The main body of the satellite is a rather stiff structure which has been modeled as a rigid body; the flexible appendages consist of a driven solar array at the far end of a boom, which is rigidly attached to the main body. The flexible array is rotated, at orbital rate, about an axis parallel to the spacecraft pitch body axis by a motor-drive system, which is mounted between the boom and the array. The overall spacecraft system, therefore, is comprised of four closed loops, i.e., pitch, roll, and yaw attitude control plus a solar-array drive servo.

The solar array consists of eight panels; however, its moment of inertia about the a_2 axis (Fig. 1) accounts for only 1% of the total spacecraft yaw or roll inertia. Hence, to facilitate the initial design effort, the array was first modeled as a beam, with its longitudinal axis aligned with a_2. The flexibility of the shaft (boom and array mast), the mounting support, and the main spacecraft body were, of course, included in the structural analysis. Although the torsional modes of the array about a_2 were also included during the design refinement phase, this structural model improvement did not result in any noticeable changes in control loop performance.

Because of the flexible appendages, stability analyses based on rigid body approximations and/or on a single, uncoupled control-axis approach do not provide the servo designer with valid results for predicting on-orbit attitude control stability margins. Since the spacecraft pitch, roll, and yaw body axes are not principal axes (i.e., large product of inertia terms exist), the resultant cross-coupling effects must be included in any meaningful analysis. Furthermore, the relative array rotation introduces additional cross-coupling effects between the control axes.

The control system performance requirements in terms of actual pointing accuracy, jitter, etc., are beyond the scope of this paper. However, it can be stated here that these requirements made it mandatory to optimize, by an iterative process, the selection of the control loop design parameters (e.g., gain and bandwidth). As a result, minimum pointing error and jitter sensitivity to internal and external disturbances were achieved, consistent with the flexible structure and interaxis cross-coupling effects.

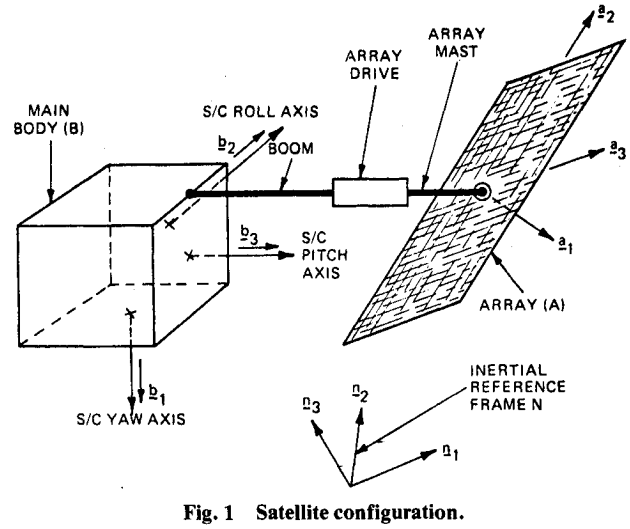

Fig. 1 Satellite configuration.

Presented as Paper 74-1262 at the CASI/AIAA Joint Meeting, Toronto, Canada, October 30-31, 1974; Submitted November 29, 1974; revision received May 2, 1975. This work was performed for the Department of the Air Force (SAMSO) under Contract F04701-72-C-0221.

Index categories: Spacecraft Attitude Dynamics and Control; Earth Satellite Systems, Unmanned.

*Senior Engineer, Astro-Electronics Division. Member AIAA.

†Manager, Attitude Control, Astro-Electronics Division. Member AIAA.

To provide an engineering design tool which takes cognizance of cross-coupling and flexible body effects, a computer program (four-loop) was developed which permits the servo designer to verify open- and closed-loop stability in terms of frequency response for any one of the four loops; i.e., either with the other three loops closed or with any one or more open (Fig. 2). The array angle is treated as a distinct input parameter so that its impact on the control system performance can be assessed. In addition, the frequency response of any control loop to external (e.g., solar-pressure and gravity-gradient torques) and internal (e.g., payload equipment and/or array-motor-cogging torque) disturbances may also be computed. The computer output consists of Bode plots in addition to printouts of gain (in decibels) and phase (in degrees) vs frequency (in rad/sec).

In view of the system complexity and its high dimension, the large number of parametric combinations (including structural characteristics), and the necessity of small time-step size, the eigenvalue and time-simulation approach was not chosen as a design tool. Once the design was iteratively arrived at by means of the multiloop frequency-response technique, it became economically feasible to examine the control response and the nonlinear characteristics by means of a time simulation.

In this particular application, the so-called "hybrid-coordinate"[4] formulation has been adopted in deriving the dynamical equations of the spacecraft system. These equations are then fully linearized with respect to a nominal state for the control analysis. A modal coordinate transformation and truncation technique[4] was applied to reduce the dimensions of the problem. In the four-loop computer program, any number up to 12 modal coordinates are allowed. Furthermore, for each of the control loops, the gains and transfer functions of components and compensation networks were utilized as input to the computer program.

To gain some physical insight concerning the interaction between the attitude control system and the spacecraft structural flexibility, the passive structural system frequencies and corresponding mode shapes of the entire spacecraft were computed first. Furthermore, the relative magnitude of the participation factor of each mode in the attitude control loop of interest was obtained. This information was essential in the control system design process because it provided additional requirements for the selection of each control loop bandwidth as well as for the resolution and range of the frequency scan. It must be understood, however, that the structural model may contain significant uncertainties, and these should be removed by actual modal tests of the structure.

Multiloop Servo Definition

In this particular application, pitch, roll, and yaw attitude control torques are supplied by three reaction wheels, i.e., one per spacecraft control axis. The blocks making up the reaction wheel servo loops are shown in Fig. 3a and defined, in terms of their transfer functions, in Table 1. It should be noted that the representation of the computational delay (i.e., a transportation lag) and the sample-and-hold blocks in exponential form by conventional Laplace transforms, rather than by z-transforms, is valid, since the sampling and delay frequencies are considerably higher than any of the control loop bandwidths. The integral control terms are inhibited to assure stability under saturated conditions. The array-drive servo block diagram is shown in Fig. 3b with the block transfer functions also defined in Table 1. All structural coupling effects between control axes are included in the dynamics transfer function (H_i), which may also contain, at the user's option, the control-system transfer functions for all other loops except the one under consideration

From the block diagrams of Fig. 3 and the definitions of Table 1, it is evident that the open-loop transfer function for any control axis i ($i=1, 2, 3, 4$) is given by

$$\theta_{si}/\theta_{\epsilon i} = G_i H_i \qquad (1)$$

where

$$\left.\begin{aligned} G_i &= G_{il} G_{i2} \\ G_{il} &= G_D G_{i0} G_W; \\ G_{i2} &= G_G G_F G_S \end{aligned}\right\} \quad i = \begin{cases} 1 \text{ (yaw)} \\ 2 \text{ (roll)} \\ 3 \text{ (pitch)} \end{cases}$$

$$\left.\begin{aligned} G_{il} &= G_{41} \\ G_{12} &= G_{42} \end{aligned}\right\} \quad i = \quad 4 \text{ (array)}$$

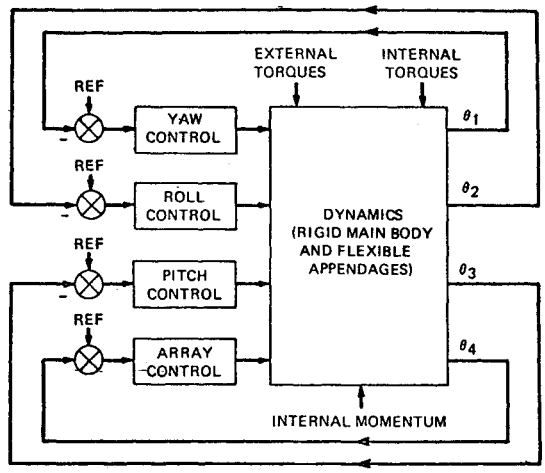

Fig. 2 Four-loop block diagram.

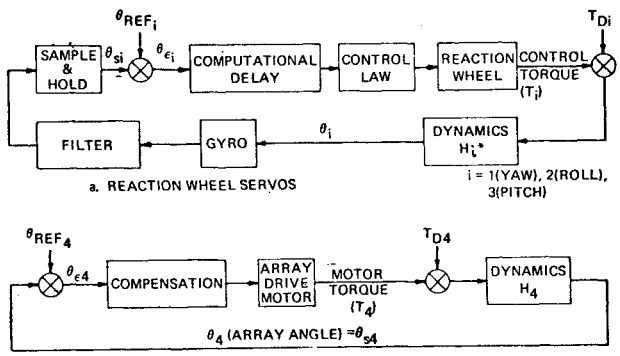

*THE CONTROL SYSTEM TRANSFER FUNCTIONS OTHER THAN THAT OF THE i^{th} LOOP ARE FULLY INCLUDED IN H_i ($i = 1, 2, 3, 4$) AT THE USER'S OPTION.

Fig. 3 Multiloop servo block diagram.

Table 1 Definition of transfer functions

Block	Transfer function
Gyro	$G_G = 1/(s^2/\omega_0^2 + 2\zeta s/\omega_0 + 1)$
Filter	$G_F = (1+as+bs^2)/(1+as+bs^2+cs^3+ds^4)$
Sample and Hold	$G_s = (1-e^{-T_s s})/(T_s s)$
Computational delay	$G_D = e^{-T_D s}$
Control law	
a) Yaw	$G_{10} = K_{11} + K_{12}s + K_{13}/s$
b) Roll	$G_{20} = K_{21} + K_{22}s + K_{23}/s$
c) Pitch	$G_{30} = K_{31} + K_{32}s + K_{33}/s + K_{34}/s^2$
Reaction wheel	$G_W = K_W s/(1+T_W s)$
Array drive (Compensation and drive motor in cascade)	$G_4 = G_{41} + G_{42}$ where $G_{41} = K_{41}(1+T_{41}s)^3/[(1+T_{42}s)^2(1+T_{43}s)(1+T_{44}s)(1+T_{45}s)(1+T_{46}s)]$ $G_{42} = K_{42}s$ (motor back EMF term)
Dynamics (includes all coupling)	$H_i = \theta_i/T_i$

Table 2 Dynamics transfer functions for various loops

Transfer function	Definition	Description
θ_1/T_1	H_1	Yaw response to yaw wheel torque
θ_2/T_2	H_2	Roll response to roll wheel torque
θ_3/T_3	H_3	Pitch response to pitch wheel torque
θ_4/T_4	H_4	Array response to array motor torque
θ_3/T_{D_4}	H_5[a]	Pitch response to array motor disturbance torque
θ_4/T_{D_2}	H_6[a]	Array response to roll axis payload disturbance torque

[a] All four control loops are closed and included in H_5 or H_6.

It follows that the closed-loop transfer function for any control axis i is given by

$$\theta_i/\theta_{Ref_i} = G_{il}H_i/(1+G_iH_i) \tag{2}$$

Furthermore, the sensitivity to a disturbance torque applied along the ith axis (T_{D_i}) is given by

$$\theta_i/T_{D_i} = H_i/(1+G_iH_i) \tag{3}$$

For the dynamic analysis to proceed, it is, therefore, necessary to develop the dynamics transfer functions H_i (i = 1, 2, 3, 4). In addition, to evaluate the effect of payload and reaction-wheel drive motor disturbance torques, it is also required to derive certain other transfer functions H_5 and H_6. Table 2 defines and summarizes the various transfer functions utilized in the design analysis. The derivation of these transfer functions requires the formulation of a set of linearized dynamical equations of the spacecraft system.

Linearized Dynamical Equations

In order to describe the system dynamical equations of the spacecraft shown in Fig. 1, the following reference frames, unit vector arrays,[4] and coordinates are defined:

N-frame	= fixed in inertial space
B-frame	= fixed in spacecraft rigid central body
A-frame	= fixed in the undeformed solar array
$[\boldsymbol{n}]^T=(\boldsymbol{n}_1,\boldsymbol{n}_2,\boldsymbol{n}_3)$	= right-handed, mutually perpendicular unit vector array fixed in N
$[\boldsymbol{b}]^T=(\boldsymbol{b}_1,\boldsymbol{b}_2,\boldsymbol{b}_3)$	= right-handed, mutually perpendicular unit vector array fixed in B
$[\boldsymbol{a}]^T=(\boldsymbol{a}_1,\boldsymbol{a}_2,\boldsymbol{a}_3)$	= right-handed, mutually perpendicular unit vector array fixed in A
$\omega_i^b (i=1,2,3)$	= scalar b_i-component of inertial angular velocity of B
β	= relative angle between A and B about $\boldsymbol{b}_3$
ϕ	= deviation of array angle from a constant β^*, i.e., $\beta=\beta^*+\phi$
ϕ_3	= twist angle of boom tip (at array drive) relative to B about $\boldsymbol{b}_3$
$\eta_i (i=1,2,\ldots,J)$	= ith appendage modal coordinate (appendage deformations are defined in $[\boldsymbol{a}]$)
$\psi_i (i=1,2,3)$	= relative angle between the ith reaction wheel and B about $\boldsymbol{b}_i$
$\epsilon_i (i=1,2,3)$	= diviation of wheel angle, i.e., $\psi_i=\psi_i^*+\epsilon_i$, $\psi_i^*=\dot{\psi}_i^* t$, $\dot{\psi}_i^*$ is a constant for $i=1,2,3$

The formulation strategy in deriving the equations of motion follows the so-called "hybrid-coordinate" approach, as outlined in Ref. 4. Three major assumptions employed in the formulation are: a) infinitesimal appendage elastic deformations in $[\boldsymbol{a}]$; b) a force-free environment; and c) ignoring the spacecraft mass center motion with respect to B due to the appendage deformations. The first two assumptions are self-explanatory. In regard to the third assumption, the mass center motion due to appendage deformations ($\boldsymbol{c}$ in Ref. 4) is a linear combination of the appendage deformations premultiplied by the ratio between the appendage mass and the total spacecraft mass. This ratio for the spacecraft under consideration is below 0.08. Since the appendage elastic deformations are assumed infinitesimal from the outset, the term $\boldsymbol{c}$ can then be considered having higher order effect. It is, therefore, ignored in the formulation. Linearization of the nonlinear dynamical equations with respect to the nominal state of interest, i.e.,

$$\omega_i^b = 0 \quad \text{for } i=1,2,3 \tag{4a}$$

$$\beta=\beta^* \quad \text{(constant)} \tag{4b}$$

$$\phi_3 = 0 \tag{4c}$$

$$\text{for } i=1,2,\ldots,j \tag{4d}$$

$$\dot{\psi}_i=\dot{\psi}_i^* \quad \text{(constant) for } i=1,2,3 \tag{4e}$$

leads to the following set of matrix differential equations:

$$\underset{3\times3}{a^\omega}\ \underset{3\times1}{\dot{\omega}^b} + \underset{3\times3}{a^g}\ \underset{3\times1}{\omega^b} + \underset{3\times1}{a^\phi}\ \underset{1\times1}{\ddot{\phi}} + \underset{3\times3}{a^\epsilon}\ \underset{3\times1}{\ddot{\epsilon}} + \underset{3\times j}{a^\eta}\ \underset{j\times1}{\ddot{\eta}} + \underset{3\times1}{a^3}\ \underset{1\times1}{\ddot{\phi}_3} = \underset{3\times1}{T^b} \tag{5}$$

$$\underset{1\times3}{b^\omega}\ \underset{3\times1}{\dot{\omega}^b} + \underset{1\times1}{b^\phi}\ \underset{1\times1}{\ddot{\phi}} + \underset{1\times j}{b^\eta}\ \underset{j\times1}{\ddot{\eta}} = \underset{1\times1}{T_\phi} \tag{6}$$

$$\underset{j\times3}{C^\omega}\ \underset{3\times1}{\dot{\omega}^b} + \underset{j\times1}{C^\phi}\ \underset{1\times1}{\ddot{\phi}} + \underset{j\times j}{M}\ \underset{j\times1}{\ddot{\eta}} + \underset{j\times j}{C}\ \underset{j\times1}{\dot{\eta}} + \underset{j\times j}{K}\ \underset{j\times1}{\eta} = \underset{j\times1}{F^\eta} \tag{7}$$

$$\underset{3\times3}{d^\omega}\ \underset{3\times1}{\dot{\omega}^b} + \underset{3\times3}{d^\epsilon}\ \underset{3\times1}{\ddot{\epsilon}} = \underset{3\times1}{T^\epsilon} \tag{8}$$

$$\underset{1\times3}{g^\omega}\ \underset{3\times1}{\dot{\omega}^b} + \underset{1\times1}{m_3}\ \underset{1\times1}{\ddot{\phi}_3} + \underset{1\times1}{d_3}\ \underset{1\times1}{\dot{\phi}_3} + \underset{1\times1}{k_3}\ \underset{1\times1}{\phi_3} = \underset{1\times1}{T_3^\phi} \tag{9}$$

A few remarks of general interest concerning the physical significance of these equations are in order. The dimension of each matrix is indicated in the equations. The coordinate matrices, e.g., ω^b, ϵ, and η are defined as:

$$\omega^{b^T} = (\omega_1^b,\ \omega_2^b,\ \omega_3^b) \tag{10a}$$

$$\epsilon^T = (\epsilon_1,\ \epsilon_2,\ \epsilon_3) \tag{10b}$$

$$\eta^T = (\eta_1,\ \eta_2,\ \ldots,\ \eta_j) \tag{10c}$$

The three scalar equations in Eq. (5) describe the rotational motion of the entire spacecraft system with respect to its mass center under the external torques T_i^b about $\boldsymbol{b}_i$ ($i=1,2,3$). The symbol a^ω denotes the spacecraft inertia matrix with respect to the $[\boldsymbol{b}]$-frame at $\beta=\beta^*$ with its mass center as the reference point. The term a^g represents the gyroscopic effect from the nominal angular momentum, h°, i.e.,

$$a^g = -\begin{bmatrix} 0 & -h_3^\circ & h_2^\circ \\ h_3^\circ & 0 & -h_1^\circ \\ -h_2^\circ & h_1^\circ & 0 \end{bmatrix} \tag{11}$$

where

$$h_i^\circ = J_i\dot{\psi}_i^* \qquad \text{for } i=1,2,3 \tag{12}$$

J_i^r is the spin inertia of the ith wheel. Other terms in Eq. (5) correspond to the contributions arising from various components of the system, i.e., solar array (ϕ and η), wheels (ϵ), and the boom twisting (ϕ_3). Equation (6) describes the rotational motion of the solar array about the motor bearing axis under the torque T_ϕ. Equation (7) depicts the array deformation motions with F^η containing the generalized forces associated with the appendage modal coordinates η_i's. Equation (8) is associated with the rotational motions of the wheels about their symmetry axes under the torque T^ϵ. Equations (9) describes the twisting motion of the boom under the torque $T_3{}^\phi$.

Transfer Functions

The nominal state of interest [Eq. (4)] implies that B is nominally stationary in inertial space. Under such a condition, it is possible to approximate ω^b as

$$\omega^b \approx \dot{\gamma} \tag{13}$$

where

$$\dot{\gamma} = \frac{\mathrm{d}}{\mathrm{d}t}\gamma = \frac{\mathrm{d}}{\mathrm{d}t}\begin{Bmatrix}\gamma_1\\ \gamma_2\\ \gamma_3\end{Bmatrix} \tag{14}$$

with $\gamma_i (i=1, 2, 3)$ denoting a 1-2-3 (yaw-roll-pitch) set of attitude angles of B about b_i's. Substitution of Eqs. (13) and (14) into Eqs. (5) to (9) provides, upon Laplace Transform and a matrix condensation process

$$Q\theta = F \tag{15}$$

where

$$\theta = \begin{Bmatrix}\theta_1\\ \theta_2\\ \theta_3\\ \theta_4\end{Bmatrix} = \begin{Bmatrix}\gamma_1\\ \gamma_2\\ \gamma_3\\ \phi - \phi_3\end{Bmatrix} \tag{16}$$

Q is a complex 4×4 matrix, and F's dimension is 4×1. Both Q and F are functions of the Laplace variable s. The control torques T_i^ϵ $(i=1, 2, 3)$ and T_ϕ are absorbed in F. Defining the 4×1 control torque matrix T by

$$T = \begin{Bmatrix}T_1^\epsilon\\ T_2^\epsilon\\ T_3^\epsilon\\ T_\phi\end{Bmatrix} \tag{17}$$

one can construct the following transfer functions from Eq. (15) for the attitude control analysis

$$H_{ij}{}^\ddagger = \theta_i / T_j \quad i, j = 1,2,3,4 \tag{18}$$

The transfer functions H_{ij}'s are formulated in such a way that the other three control loops are included in the expressions, i.e., replacing $T_\alpha (\alpha \neq j)$ by $-(G_\alpha \theta_\alpha)$ where $G_\alpha (\alpha = 1,2,3,4)$ contains the control law and other relevant hardware characteristics as defined earlier. In constructing the transfer function, H_5 and H_6 (Table 2), all four control loops are closed. In view of the complex nature of these transfer functions, they are not expanded into explicit polynomials in the s-variable. Instead, a frequency response computer program called "four-loop" is formulated to determine numerically the phase and gain of various open- and closed-loop transfer functions, discretely scanning through a frequency range of interest. The stability margins can then be established via Nyquist diagrams directly plotted from the four-loop output.

‡In Table 2, H_{ii} has been simply denoted by H_i for $i=1, 2, 3, 4$.

Results

The frequency-domain analysis for the particular spacecraft control being investigated shows roll and yaw coupling effects to be small. The pitch loop, however, exerts considerable influence on the solar-array drive and vice versa. Furthermore, strong coupling is also indicated between pitch and yaw because of the prevailing mass distribution.

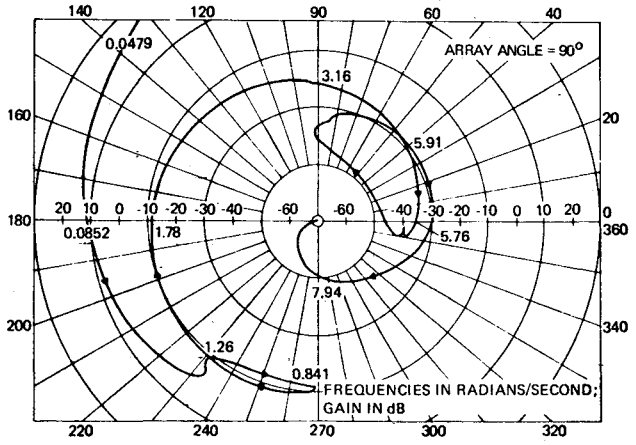

Fig. 4 Pitch open-loop Nyquist diagram (all other loops closed).

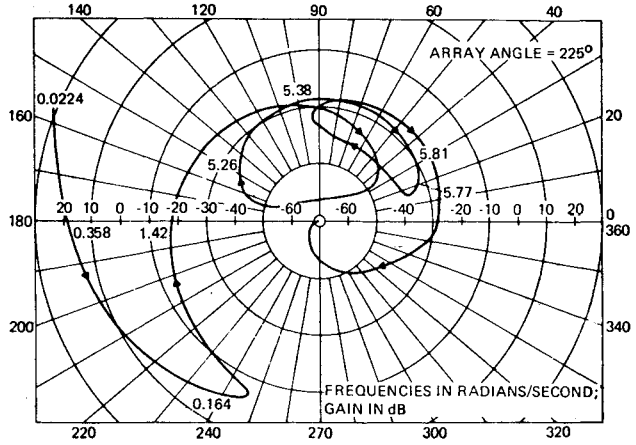

Fig. 5 Roll open-loop Nyquist diagram (all other loops closed).

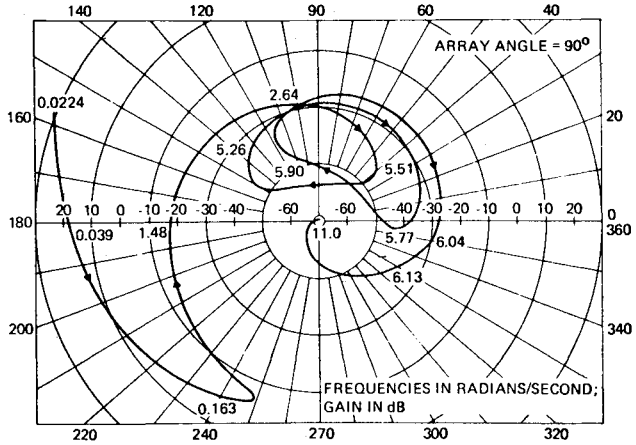

Fig. 6 Yaw open-loop Nyquist diagram (all other loops closed).

In general, the system modes are very complex, due to their dependence on the array orientation with respect to the main body. The first system mode accounts primarily for the bending of the boom and the array mast, with the slightly deformed solar array moving in the $\pm a_2$ direction and the main body moving as a rigid body. The second system mode can be described by the bending of the boom and the array mast with a symmetrically bent array (about a_3) and a moving rigid main body; higher modes are more complex.

The interaction between the control loops and the structural flexibility is vividly demonstrated by the Nyquist diagrams of Figs. 4-9. The pitch loop Nyquist plot of Fig. 4 shows array loop coupling at the 0.841 rad/sec inversion. The first structural mode of 5.4 rad/sec has insignificant influence on this axis, whereas the effects of the second structural mode of 5.9 rad/sec are clearly evident. Higher frequency resonances are either attenuated by filtering or only weakly coupled into the pitch axis. Although only one array-angle plot (in this case for 90°) is included here for illustrative purposes, the design study involved the examination of the complete range of on-orbit array positions. The pitch loop, as well as the roll and yaw loops, are of a gain-stable design.

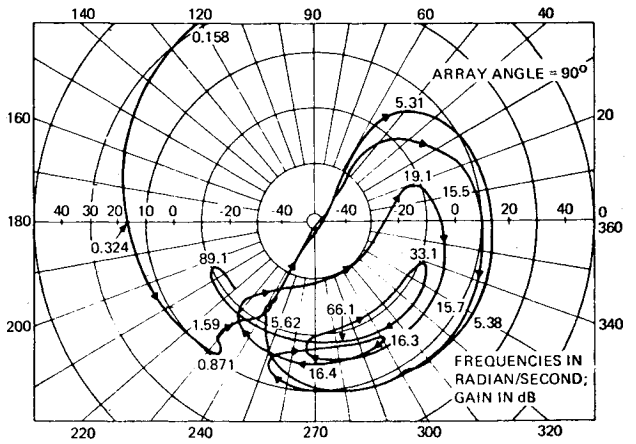

Fig. 7 Array open-loop Nyquist diagram (all other loops closed).

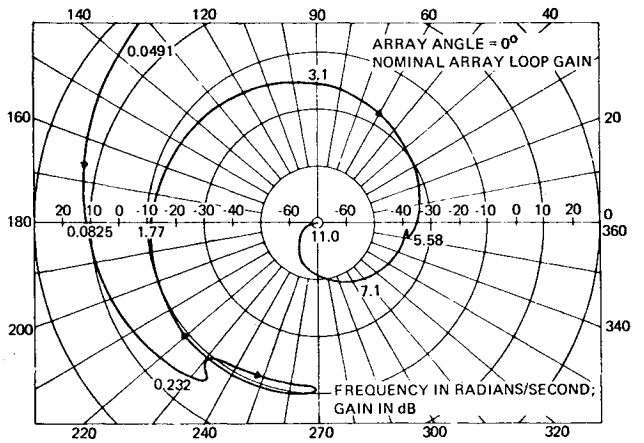

Fig. 8 Pitch open-loop Nyquist diagram (all other loops closed), nominal array loop gain.

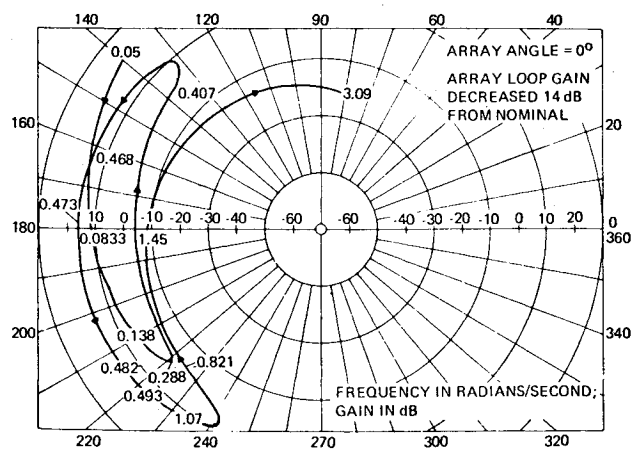

Fig. 9 Pitch open-loop Nyquist diagram (all other loops closed), decreased array loop gain.

The plot of the roll loop (Fig. 5) shows the effects of flexible body coupling of the first and second mode between 5.38 and 5.77 rad/sec. Higher modes are either weakly coupled or are suppressed by filtering. The yaw loop plot of Fig. 6 indicates similar performance. Bandwidth and gain in all cases is sufficiently high to counteract various disturbances due to tape recorders, magnetic torques, gyroscopic coupling, gravity gradient, and solar torques.

The Nyquist plot of Fig. 7 illustrates the fact that the solar-array drive loop is conditionally stable, i.e., a decrease in gain can cause instability. Since adequate bandwidth is required both in the array and the pitch loop to counteract the cogging torque effects of the array drive motor, a phase-stable design is necessary for this fourth loop. Saturation conditions, which represent reduction in gain and consequently in stability, were thoroughly investigated to assure satisfactory performance under all circumstances. The plot shows strong coupling with the first (5.40 rad/sec), third (16.1 rad/sec), and fifth (30.3 rad/sec) structural modes.

Because of the strong coupling, careful attention to parametric variations and saturation effects has to be given to the pitch loop when examining array-loop stability, and vice versa. The computer program calculates the integral of the square of the magnitude of the pitch response to the solar-array motor disturbance torque transfer function. Thus, for a given power-spectral-density torque noise, the pitch response can readily be determined.

To verify the stability margin and the coupling between the pitch and array loops, the nominal array gain was reduced by 14 db, with the comparative pitch loop results shown in Figs. 8 and 9. Obviously, such a drastic gain reduction causes an unstable condition in the pitch loop. The corresponding parameters were subsequently examined in the time-domain simulation, which confirmed the prediction of the Nyquist plots.

Conclusions

As demonstrated by the DMSP example presented in this paper, the four-loop program is a valuable design tool, providing substantial computer time savings as compared to other approaches. In the four-loop program, the computation includes two separate matrix inversions. The first one occurs during the condensation process; i.e., expressing η in terms of θ and ϕ from Eq. (7). Since M, C, and K are diagonal, the inversion of the sum of these matrices is simply obtained by inverting each of its diagonal elements. A second inversion of the 4×4 Q-matrix [Eq. (15)] is required in computing the H_i's. In view of the simplicity of the first inversion and the small size of Q, the frequency response approach is very direct and economical, as compared with the eigenvalue analysis of the complete system. However, in addition to the directness and economy of the methodology utilized for the four-loop program, its primary utility lies in its application to the synthesis and analysis of multiloop spacecraft control systems with controlled flexible appendages, where a single-axis analysis could lead to an unacceptable (and possibly catastrophic) design.

References

[1] Hooker, W. W. and Margulies, G., "The Dynamical Attitude Equations for an N-body Satellite," *Journal of Astronautical Sciences*, Vol. 12, Winter, 1965, pp. 123-128.

[2]Pringle, R., Jr., "On the Stability of a Body with Connecting Moving Parts," *AIAA Journal*, Vol. 4, Aug. 1966, pp. 1395-1404.

[3]Roberson, R. E. and Wittenberg, J., "A Dynamical Formalism for an Arbitrary Number of Interconnected Rigid Bodies with Reference to the Problem of Satellite Attitude Control," *Proceedings of the Third International Congress of Automatical Control*, Butterworth, London, 1967.

[4]Likins, P. W., "Dynamics and Control of Flexible Space Vehicles," Rev. 1, Jan. 15, 1970, *Jet Propulsion Lab.*, TR 32-1329, Pasadena, Calif.

[5]Vigneron, F. R., "Stability of a Freely Spinning Satellite of Crossed-Dipole Configuration," *Transactions of the Canadian Aeronautics and Space Institute*, Vol. 3, March 1970, pp. 8-19.

[6]Mingori, D. L., "A Stability Theorem for Mechanical Systems with Constraint Damping," *Journal of Applied Mechanics*, June 1970, pp. 253-258.

[7]Grote, P. B., McMunn, J. C., and Gluck, R., "Equations of Motion of Flexible Spacecraft," *Journal of Spacecraft and Rockets*, Vol. 8, June 1971, pp. 561-567.

[8]Meirovitch, L., "A Method for the Lyapunov Stability Analysis of Force-Free Dynamical Systems," *AIAA Journal*, Vol. 9, Sept. 1971, pp. 1695-1701.

[9]Kulla, P., "Dynamics of Spinning Bodies Containing Elastic Rods," *Journal of Spacecraft and Rockets*, Vol. 9, April 1972, pp. 246-253.

[10]Hughes, P. C., "Attitude Dynamics of a Three-Axis Stabilized Satellite with a Large Flexible Solar Array," *Journal of Astronautical Sciences*, Vol. XX, Nov.-Dec. 1972, pp. 166-189.

[11]Tseng, G. T., "Dynamical Equations of Spacecraft with Controlled Flexible Appendages Using Finite Element Appraoch," AIAA Paper No. 74-1261, *CASI/AIAA Joint Meeting*, Toronto, Ont., Can., Oct. 30-31, 1974.

[12]Gale, A. H. and Likins, P.W., "Influence of Flexible Appendages on Dual-Spin Spacecraft Dynamics and Control," *Journal of Spacecraft and Rockets*, Vol. 7, Sept. 1970, pp. 1049-1056.

[13]Porcelli, G., "Attitude Control of Flexible Space Vehicles," *AIAA Journal*, Vol. 10, June 1972, pp. 807-812.

[14]Marsh, E. L., "Attitude Stability of a Flexible Solar Electric Spacecraft," *Journal of Spacecraft and Rockets*, Vol. 11, Feb. 1974, pp. 89-96.

[15]Larson, V., "Suboptimal Controller for a Linearized *n*-Body Spacecraft," *Journal of Spacecraft and Rockets*, Vol. 2, Dec. 1974, pp. 858-860.